Evolutionary method for predicting surface reconstructions with variable stoichiometry

Qiang Zhu,[1,2,*] Li Li,[3] Artem R. Oganov,[1,2,3,4] and Philip B. Allen[3]

[1]*Department of Geosciences, Stony Brook University, Stony Brook, New York 11794, USA*
[2]*Center for Materials by Design, Institute for Advanced Computational Science, Stony Brook University, New York 11794, USA*
[3]*Department of Physics and Astronomy, Stony Brook University, Stony Brook, New York 11794, USA*
[4]*Department of Problems of Physics and Energetics, Moscow Institute of Physics and Technology, 9 Institutskiy Lane,
Dolgoprudny city, Moscow Region, 141700, Russia*

We present a specially designed evolutionary algorithm for the prediction of surface reconstructions. This technique allows one to automatically explore stable and low-energy metastable configurations with variable surface atoms and variable surface unit cells through the whole chemical potential range. The power of evolutionary search is demonstrated by the efficient identification of diamond 2×1 (100) and 2×1 (111) surface reconstructions with a fixed number of surface atoms and a fixed cell size. With further variation of surface unit cells, we study the reconstructions of the polar surface MgO (111). Experiment has detected an oxygen trimer (ozone) motif [Plass *et al.*, Phys. Rev. Lett. **81**, 4891 (1998)]. We predict another version of this motif which can be thermodynamically stable in extreme oxygen-rich conditions. Finally, we perform a variable stoichiometry search for a complex ternary system: semipolar GaN ($10\bar{1}1$) with and without adsorbed oxygen. The search yields a counterintuitive reconstruction based on N_3 trimers. These examples demonstrate that an automated scheme to explore the energy landscape of surfaces will improve our understanding of surface reconstructions. The method presented in this paper can be generally applied to binary and multicomponent systems.

PACS number(s): 68.43.Bc, 31.15.E−

I. INTRODUCTION

At crystalline surfaces, especially in semiconductors, atoms rearrange to form reconstructed configurations, which are different from those in the bulk crystals. Reconstructions play a key role in surface properties and behaviors, such as epitaxial crystal growth, catalysis, etc. Determination of the reconstruction of semiconductor surfaces is a long-standing problem. Despite progress in experimental techniques, it is still hard to obtain the atomic-scale details. Diffraction and microscopy can yield the periodicity and symmetry.[1,2] However, the sampling space is astronomically large, and solutions may defy intuition, even for monatomic systems: consider Si(111) 7×7 reconstruction.[3–5] For binary and more complex cases, a variable stoichiometry at the surface adds a huge extra dimension. The problematic complexity of surface structures is further compounded by a range of synthesis techniques. Varying precursor compounds of possibly mixed gas, liquid, or solid phases, varying pressures and temperatures during synthesis, varying annealing schedules, etc., may allow a significant range of metastable surface phases to survive. Thus experiments may correctly offer conflicting suggestions about structure. Therefore theory has a role not just in attempting to predict true thermodynamically stable structures, but also in cataloging potential metastable phases, needed for guidance in interpretation of experiment.

From the computational perspective, the main difficulty lies in the fact that the number of candidate structures is extremely large. It is not possible to enumerate all the reasonable reconstruction models just from chemical intuition. There have been a few efforts towards automatic prediction of the most stable configuration for either a given stoichiometry[6–8] or a variable composition at constant chemical potential.[9] With these structural models available, the surface phase diagram can be constructed.[10] However, unbiased prediction of reconstructions with variable stoichiometry in the whole chemical potential range has not been attempted to our knowledge. Here we demonstrate that the unbiased nature of an evolutionary search is able to find unexpected structures that compete thermodynamically with ones already suggested by prior searches. In this paper, we propose a method which allows automatic exploration of stable and low-energy metastable configurations, with variable surface atoms and variable reconstruction cells through the whole chemical potential range. We apply this method to a series of systems: diamond (100) and (111), MgO (111), and GaN ($10\bar{1}1$) surfaces with and without added oxygen.

II. THEORETICAL BACKGROUND

A. Surface energy and chemical potential

Relative stability among candidate surfaces is determined by the formation energy $E_{\text{formation}}$,

$$E_{\text{formation}} = E_{\text{tot}} - E_{\text{ref}} - \sum_i n_i \mu_i, \tag{1}$$

where E_{tot} and E_{ref} are the total energy of the surface under consideration and of the reference cleaved surface; n_i and μ_i are the number (in excess of the cleaved surface) and chemical potential for each species, respectively. The chemical potential is the energy needed to add or remove one atom from the system, assuming there is a reservoir for each species to equilibrate with. The chemical potentials must satisfy constraints. For a simple binary AB compound, if μ_A is extremely high, the elemental phase A would condense on the substrate AB. Therefore, the chemical potential of A (or B) is upper bounded by the chemical potential of elemental A (or B),

$$\mu_A \leqslant \mu_A^0, \quad \mu_B \leqslant \mu_B^0. \tag{2}$$
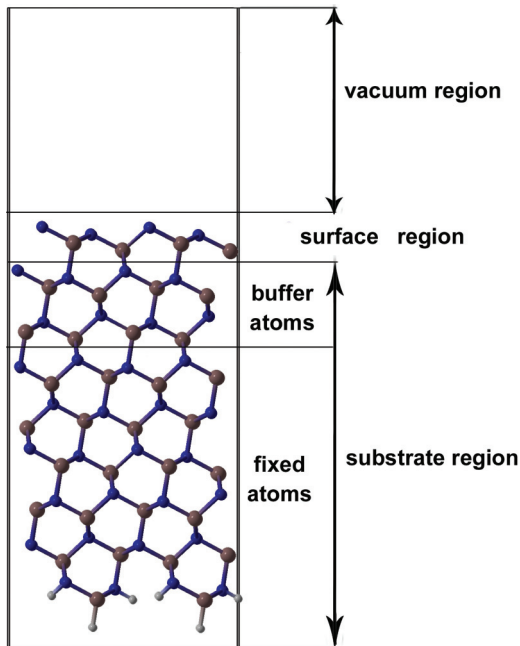
FIG. 1. (Color online) Surface representation used in the evolutionary algorithm.

The A and B atoms are in equilibrium with the substrate,

$$\mu_A + \mu_B = G_{AB}. \tag{3}$$

At $T = 0$ K, the Gibbs free energy G_{AB} reduces to the internal energy E_{AB}.

These conditions lead to a range of the A component chemical potential of

$$E_{AB} - \mu_B^0 \leqslant \mu_A \leqslant \mu_A^0. \tag{4}$$

Therefore, Eq. (1) can be rewritten as only μ_A dependent:

$$E_{\text{formation}} = E_{\text{tot}} - E_{\text{ref}} - n_B E_{AB} - \mu_A(n_A - n_B). \tag{5}$$

The surface phase diagram shows which reconstruction is favored under a specific environment, i.e., temperature and chemical potential or partial pressure of each component. Each of these environmental conditions represents an independent dimension in the phase diagram.

B. Evolutionary algorithm

We employ an evolutionary algorithm (EA) to explore the surface structures. The algorithm is implemented in the USPEX package, which has been successfully applied to various bulk materials.[11–14] We use a representation in which the system has three parts: vacuum, surface, and substrate (Fig. 1). Vacuum and substrate regions are prespecified, while the surface region is optimized by the EA. The number of surface atoms varies up to a predefined maximum number for a given thickness of surface. To allow automatic exploration of reconstructions with different surface unit cells, the cell size is also variable.

Our algorithm is constructed in the following way. It first generates random structures with only the surface region being varied. These initial structures are then relaxed and ranked by fitness, based on the energy. Structures with better fitness are
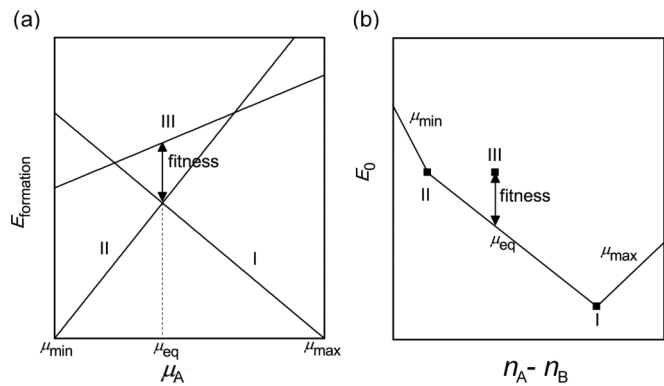

FIG. 2. Illustration of the fitness function used in the evolutionary algorithm. (a) Phase diagram as a function of μ_A. (b) Phase diagram as a function of $(n_A - n_B)$. The vertices of the convex hull are the stable structures appearing in the phase diagram. The slope of each section of the convex hull is either the boundary chemical potential or the equilibrium chemical potential where stable structures can coexist.

more likely to be selected as parents to generate new child structures. We considered three ways to produce offspring.

(i) Heredity: Two structures are chosen from the previous generation. They are randomly sliced at the same position in the surface unit cell. Then pieces from both parent structures are combined to generate the offspring.

(ii) Mutation: One structure is chosen as parent. As in the implementation of softmutation in bulk crystals,[15] the surface atoms are displaced according to the softest surface vibrational modes based on the bond-hardness model.[16,17] If the structure cannot be softmutated anymore, we switch to the coordinate mutation,[15] which is to randomly displace the surface atoms by an amount drawn from a zero-mean Gaussian distribution and biased by a specific measure of the local order.[18]

(iii) Transmutation: One structure is chosen as parent. Some atoms are transmuted to another chemical species.

The offspring, together with a few best structures from the previous generation, comprise the next generation. This process is repeated until no lower-energy structures are produced for sufficiently many generations.

C. Fitness function

Our fitness function needs to indicate the relative stability of structures with various surface stoichiometry and reconstruction cell sizes. We illustrate this in Fig. 2. First, for two given surface configurations (I and II) which have different numbers of atoms on the same substrate cell, their relative energy difference depends on the chemical potential μ_A according to Eq. (5). As shown in Fig. 2(a), surfaces I and II should coexist at $\mu_A = \mu_{\text{eq}}$. Therefore, the stability regime for the two surfaces can be fully established. Surface I is stable when $\mu_{\text{min}} \leqslant \mu_A \leqslant \mu_{\text{eq}}$, while surface II is stable when $\mu_{\text{eq}} \leqslant \mu_A \leqslant \mu_{\text{max}}$. For any other unstable configuration like surface III, the fitness can be viewed as the minimum energy difference compared with the stable configuration, at all possible chemical potentials. The minimum condition is reached when $\mu_A = \mu_{\text{eq}}$. For practical implementation it is useful to express this algebraically. We define $E_0 = E_{\text{tot}} - E_{\text{ref}} - n_B E_{AB}$ as the μ_A-independent term in Eq. (5). This approach was introduced by Qian *et al.*,[19]

and is widely used.[20] Versions (a) and (b) of Fig. 2 contain equivalent information. The stable structures appearing on the phase diagram form a convex hull in energy-composition coordinates. The slope of each section of the convex hull is either the boundary chemical potential or the equilibrium chemical potential where stable structures can coexist. We then choose the fitness of a surface structure to be its distance to the convex hull. The EA search then aims to optimize the convex hull, similarly to our previously proposed approach of variable-composition prediction for bulk crystals.[12,21] When different sizes of surface cell ($m \times n$) occur, the scale factor $N_{cell} = m \times n$ should be taken into account and energies have to be normalized.

D. Details of *ab initio* calculations

As a global optimization method, an EA search requires hundreds or thousands of individual structural relaxations. In our calculation, relaxations were done using density functional theory (DFT) within the generalized gradient approximation[22] (GGA) using the all-electron projector augmented wave[23] (PAW) method as implemented in the VASP code.[24] We used the kinetic energy cutoff of 550 eV for the plane-wave basis set and Brillouin zone sampling resolution of $2\pi \times 0.08$ Å^{-1}, which showed excellent convergence of the energy differences, stress tensors, and structural parameters. There are different ways to construct the model. If, in the point group of the crystal, surfaces (hkl) and ($\overline{hkl}$) are symmetrically equivalent, one can build a symmetric model. The other way is to passivate one surface, for example, by fractional hydrogen atoms.[25] For a semiconductor this makes the passivated surface semiconducting, with no surface states in the fundamental band gap. Dipole corrections are added in form of a mid-vacuum discontinuity in the electrostatic potential which cancels the interactions between the slab and its periodic images.[26,27] For massive calculations in EA search, we used passivated slab models. Each typical slab contains 5–7 atomic layers and 10–12 Å of vacuum, with

the top two layers being relaxed. For postprocessing, we select all high-fitness candidate structures from EA search to construct the surface stability phase diagram. To obtain accurate surface energies, we expand the slab to 8–10 layers, and the vacuum to 12–15 Å. Both symmetric models and passivation approaches were explored at this stage. Our tests suggest that the surface energy is converged to better than 0.05 eV per surface cell.

III. APPLICATIONS

In this section, we apply our method to several systems with increasing complexity. First, we study diamond (100)/(111) reconstructions by fixing both variables (number of surface atoms and cell size). For the MgO (111) surface, we focus on the particular stoichiometry (MgO) on the Mg-terminated surface, and explore the possible low-energy reconstructions with a cell size ranging from 1×1 to 2×2. Finally, we investigate the semipolar GaN ($10\overline{1}1$) surfaces without and with oxygen absorption, in which the search allows both variable surface atoms and variable surface unit cells.

A. Diamond (100) and (111)

To test our method, we applied the EA search to study the known 2×1 reconstructions of diamond (100) and (111) surfaces, which are the two most important surfaces for polycrystalline diamond obtained from chemical vapor deposition.[28] As a benchmark, we fixed the number of surface atoms and the cell size in our searches. We tried two and six carbon atoms on a 2×1 surface cell. During the search, each structure was first relaxed with the Brenner potential[29] as implemented in the GULP code,[30] and then more accurate energy evaluation was performed at the *ab initio* level with the Perdew-Burke-Ernzerhof (PBE) functional.[22]

Our results are in excellent agreement with those reported in previous literature.[28] Figure 3 shows the best structures found in the search. The cleaved diamond (100) surface, containing one unsaturated carbon atom with two dangling
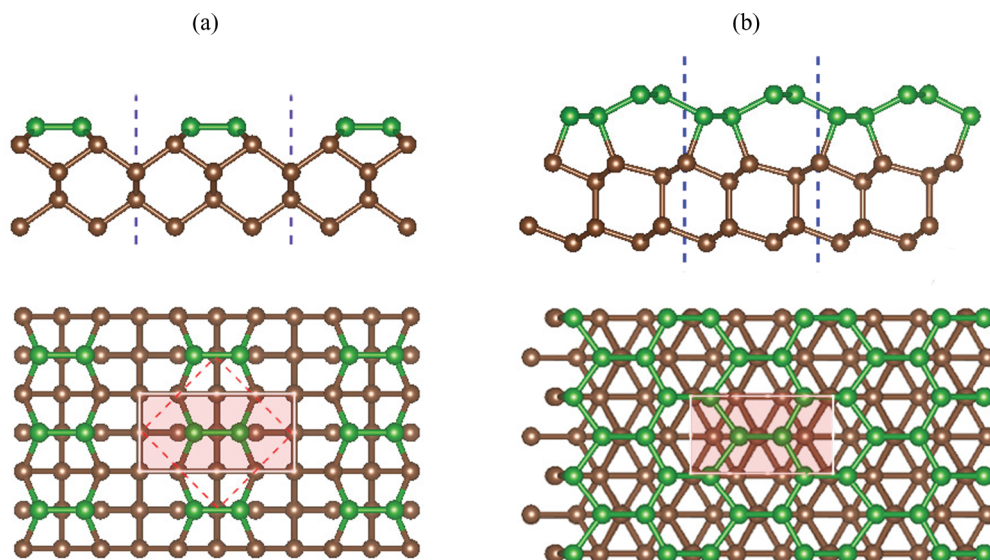

FIG. 3. (Color online) Schematic image of (a) diamond (100) 2×1 reconstruction (red dashed line, face of conventional cube); (b) diamond (111) 2×1 reconstruction. 2×1 surface unit cells are highlighted by the pink rectangle.

bonds per unit cell, is unstable. Stabilization is achieved *via* a reconstruction with surface atoms forming one π-bonded C-C dimer per 2×1 unit cell. This is correctly found by our EA search [Fig. 3(a)]. The bulk-terminated diamond (111) surface contains two unsaturated carbon atoms with two dangling bonds per 1×1 unit cell. Pandey first proposed a chain model to explain the Si (111) surface,[31] and it proved to be correct for diamond as well.[28] Our search also confirmed this model, with surface atoms forming Pandey chains along the [01$\bar{1}$] direction. From the top view [Fig. 3(b)], the Pandey chains further form an extended two-dimensional (2D) network, having the same period as the unreconstructed (111) surface. From the side view, the surface atoms together with the second layer form an alternating $(5 + 7)$-ring pattern, which is different from the 6-ring pattern in the bulk. The peculiar $(5 + 7)$-ring topology also exists in 3D in the recently established structure of a new allotrope of carbon formed by cold compression of graphite.[32,33] This demonstrates that either reduced dimensionality or extreme pressure conditions can create a very different chemical environment, leading to very complex reconstructions. Unbiased searching of these systems' landscapes is needed to find such new chemistry.

We also examined 4 and 12 carbon atoms on a 2×2 cell, but only with the Brenner potential. Although the Brenner potential gives the wrong energy ranking, the true ground states were also found as low-energy configurations in the search. With this encouragement, we proceed to the case of more than one atomic type and variable stoichiometry.

B. MgO (111)

Magnesium oxide is one of the most abundant materials in planetary mantles, and also an archetypal ionic crystal with a rocksalt-type ($B1$) structure. However, surfaces of $B1$-MgO present a challenging problem, especially for the polar (111) surface. An ideal bulk termination of the MgO (111) surface contains alternating planes of Mg^{2+} and O^{2-} ions, allowing a surface dipole along the [111] direction, leading to an extremely unstable surface configuration. To stabilize this polar (111) surface, there must be valence compensation to cancel the surface dipole, achieved either by rearrangement of surface species or by adsorption of some foreign species. Ciston *et al.*[34,35] investigated the coverage by hydroxyl (OH), combining transmission electron microscopy (TEM) and DFT calculations. They proposed several models of water-driven reconstructions. Regarding reconstruction of the clean surface, Wolf[36] proposed a 2×2 reconstruction of the $B1$-NaCl (111) surface based on valence-neutral octupolar units where 3/4 ions of the top layer and 1/4 ions of the second layer are missing, thus forming O_1-Mg_3-O_4 (O-terminated) or Mg_1-O_3-Mg_4 (Mg-terminated) surface stoichiometry. However, octupolar reconstructions are not fully consistent with the experimental data. Finocchi *et al.*[37] found a Mg-terminated phase (designated as the α-Mg phase) with a 2×2 repeating unit to be favored in O-poor conditions. They further proposed a combination of O-oct and α-Mg which could fit the diffraction data. Using transmission high-energy electron diffraction (THEED), Plass *et al.*[38] reported another major class of reconstructions on MgO (111), which is based on cyclic oxygen trimer units (2×2, $\sqrt{3} \times \sqrt{3}$, $2\sqrt{3} \times 2\sqrt{3}$).

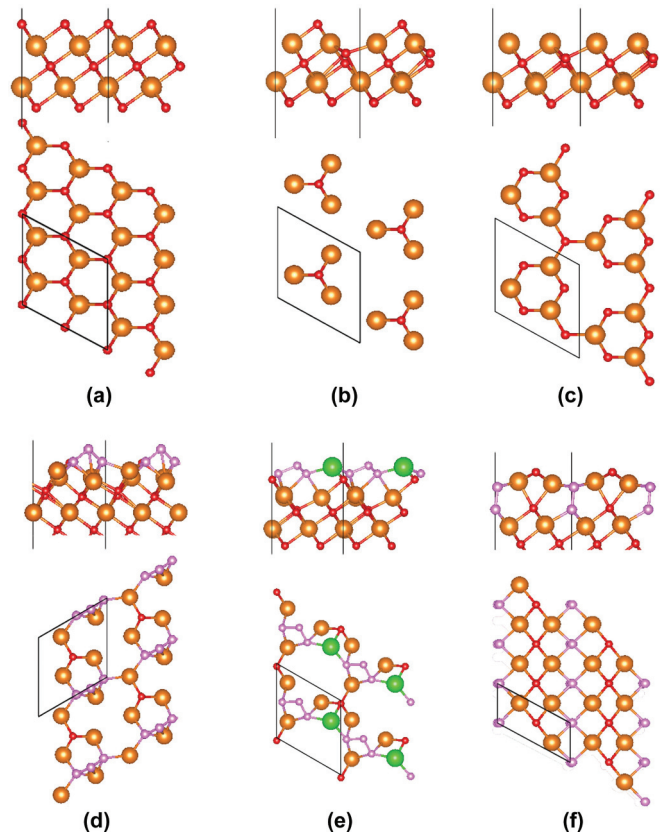FIG. 4. (Color online) Side views (top, two layers only) and top views (bottom) of MgO (111) surfaces. (a) Unreconstructed surface; (b) 2×2 O-terminated octupolar model; (c) 2×2 α-Mg model; (d) 2×2 O_3 model; (e) 2×2 Mg-O_3 model; and (f) 2×1 O_2 model. The α-Mg model can be derived by simply removing the topmost O atom from the O-terminated octupolar model. Large spheres, magnesium; small spheres, oxygen. The topmost O_3 trimers in (d), O_3-Mg-O_3 chains in (e), and peroxo O_2 species in (f) are highlighted with different colors.

DFT calculations[39] indicate that 2×2 O-octupolar reconstruction is dominantly stable over a wide oxygen chemical potential range. α-Mg is favored under Mg-rich conditions. However, the cyclic ozone 2×2 reconstruction is calculated to have much higher surface energy in the whole chemical potential range. The huge disagreement between simulation and experiment suggests that the structural model might need to be revised.

We used an EA search for the MgO (111) surface with fixed surface stoichiometry Mg_1O_1 per 1×1 cell on the given substrate (O terminated), and a variable cell size (from 1×1 to 2×2). Our search yields a low-energy reconstruction based on the O_3 trimer unit. As shown in Fig. 4(d), the topmost surface is a periodic arrangement of trimers and single oxygen atoms, which is very similar to the model suggested by Plass *et al.*[38] However, our search found a configuration with energy lower by -0.026 eV per 1×1 cell. The side view of this reconstruction [Fig. 4(e)] indicates that in each repeat unit, one Mg atom in the second layer jumps to the topmost layer, and thus leaves a Mg vacancy, displaying the same Mg_3 stoichiometry plane per 2×2 cell as in the O-octupolar model and the α-Mg model. The extra Mg atom in the top layer
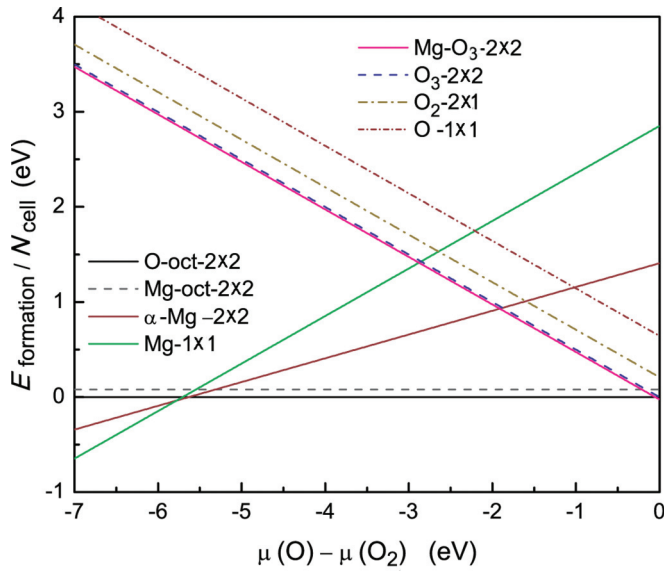
FIG. 5. (Color online) Zero-temperature phase stability diagram for the proposed reconstructions on the MgO (111) surface where $\mu(O_2) = \frac{1}{2}E(O_2)$ and $E(O_2)$ is the zero temperature energy of an O_2 molecule.

connects neighboring O_3 trimers, forming periodic O_3-Mg-O_3 chains. Thus we call it Mg-O_3-2×2.

Another interesting reconstruction appearing in our search is a 2×1 reconstruction containing the peroxo species

$[O_2]^{2-}$. This motif has the same surface stoichiometry as Mg-O_3-2×2; its surface energy is 0.23 eV per 1×1 cell higher. Although not favored on the (111) surface, it might exist on some other surfaces, such as the (100) surface.[40] This type of motif can provide a hint for experimental growth of the crystal MgO_2, which is calculated to be stable at high pressure.[41] It indicates that novel chemistry under extreme conditions (such as high pressures) might also be achieved by careful exploitation of reduced dimensionality.

Using an established way to correct for errors of the GGA functional, the calculated DFT energy of the O_2 molecule is considered to have an upward shift of about 1.05 eV.[42] Including this empirical correction, we construct the phase diagram (as shown in Fig. 5) according to Eq. (5). The phase diagram is very similar to the diagram presented in Ref. 39, except that the proposed models in our search have significantly lower energy than previous models with the same surface stoichiometry (Mg:O = 1:1). In particular, the Mg-O_3-2×2 reconstruction is calculated to be stable over a narrow range of chemical potential when O is extremely rich $[\mu(O) - \mu(O_2) \geqslant 0.06$ eV]. Given this, it is very likely that these reconstructions could be observed under certain experimental protocols.

C. GaN ($10\bar{1}1$) with and without oxygen

The applications so far use only fixed-stoichiometry searches. To prove the possibility of automated exploration of the whole stoichiometric space, we perform calculations for
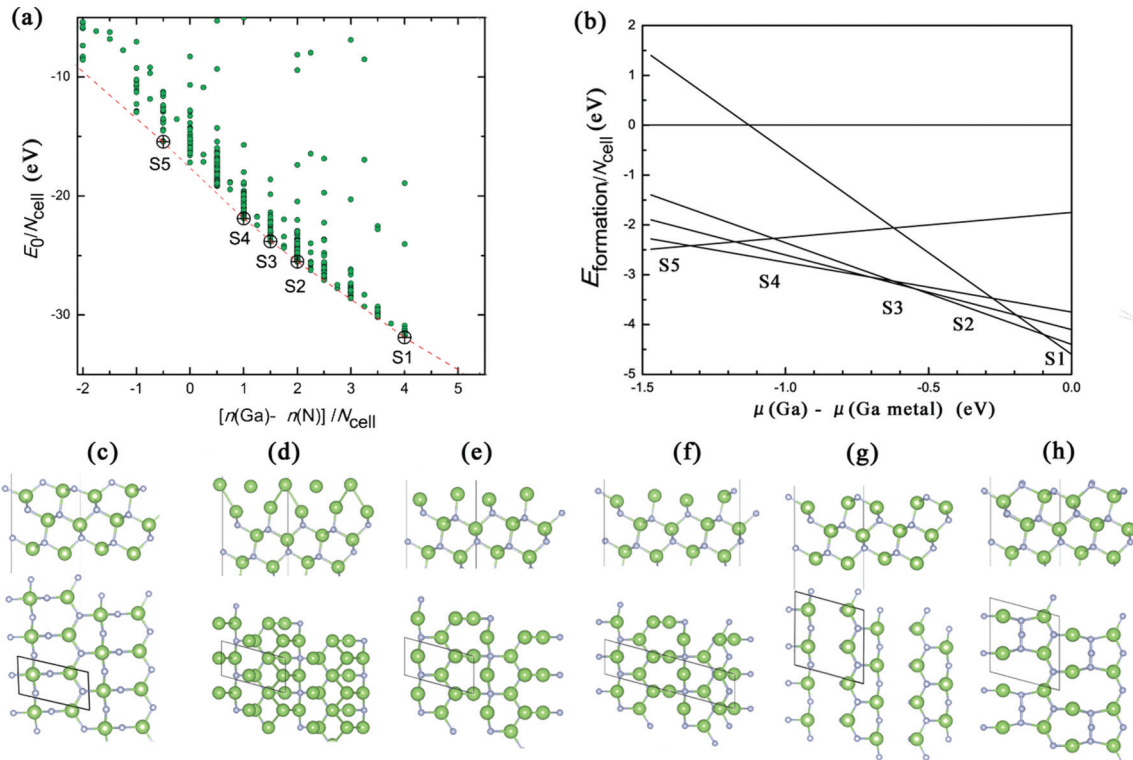

FIG. 6. (Color online) (a) Energies of GaN ($10\bar{1}1$) surface reconstructions explored by the EA search; (b) the corresponding zero-temperature phase stability diagram up to 2×2 supercell reconstructions. Side view and top view of (c) the cleaved GaN ($10\bar{1}1$) surface and its lower-energy reconstructions found by the EA search; (d) S1 configuration, (1×1) Ga bilayer; (e) S2 configuration, (1×1) Ga monolayer; (f) S3 configuration, (2×1)–1.5 N vacancy; (g) S4 configuration, (2×1)–1 N vacancy; (h) S5 configuration, (2×1) N trimer. Large spheres, gallium; small spheres, nitrogen.

the semipolar GaN $(10\bar{1}1)$ surfaces, which allows both variable surface atoms and variable cell size (restricted to a 2×2 or smaller surface cell). We also study the reconstructions on the semipolar GaN $(10\bar{1}1)$ surfaces in the presence of oxygen.

Figure 6(a) gives the convex hull diagram from our EA search, and the five corresponding stable structures. Compared to the cleaved surface [Fig. 6(c)], structure S1 has two Ga adlayers. Structure S2 has one Ga adlayer. Structure S3 has the top N and half of the second N layer removed. Structure S4 has only the top N layer removed. Structure S5 has an additional N at the bridging position of the two top N atoms. The first four structures were found by Akiyama *et al.*[43] Structure S5 with N_3 trimers is not intuitively obvious. This demonstrates the power of the automated searching by the EA. An analogous Se-trimer feature has been predicted to be stable on ZnSe (100) reconstructions in Se-rich conditions.[44] Compared to the cleaved surface, the stable structures can be constructed through either vacancies or adatoms. No more complicated reconstructions have been found. For the Ga-rich conditions, there are many intermediate structures between structures S1 and S2, lying very close to the convex hull (see Fig. 6). This can be explained by the weak directionality of the Ga-Ga bonds. These structures may appear under finite temperatures. For the N-rich conditions, however, most structures are much higher above the convex hull, due to the strong covalent bonding nature of N-N interactions.

The features possessed by the stable configurations are (i) Ga layers; (ii) N vacancies; (iii) N trimers. Another common feature is N_2 dimers.[44] These do not lie on the convex hull, but frequently appear as energetically competitive in our EA search.

The electron counting (EC) rule[45–47] emerges from the study of semiconductor surfaces. This rule, although not exact, is very useful in comparing surface energies, estimating surface charges, and guessing surface reconstructions. It states that the surface structures with filled dangling bonds on the electronegative elements and empty dangling bonds on the electron-positive elements are the lowest in energy. The surface then is likely to be semiconducting. Surfaces not satisfying this rule will be metallic and higher in energy. None of the stable reconstructions found here satisfy the electron counting rule. Large reconstructions may satisfy the EC rule. Indeed, Lee and Kim[48] demonstrated that low-energy semiconducting surfaces can be achieved by large reconstructions, complying with the EC rule by constructing models based on the N dimer and dimer vacancy. Due to the limitation of computational power, we attempt to predict the reconstructions only up to 2×2 surface cells. But our results provide a good starting point for predicting large reconstructions.

Let us now employ the same method to search for reconstructions of GaN $(10\bar{1}1)$ surfaces with added oxygen. The formation energy can be defined as

$$E_{\text{formation}} = E_0 - \mu(\text{Ga})[n(\text{Ga}) - n(\text{N})] - \mu(\text{O})n(\text{O}). \quad (6)$$

The oxygen chemical potential $\mu(\text{O})$ is a new variable. It has no lower bound, but we can formulate the upper bound by the constraints based on the possible O_2, N_xO_y molecular gas, and
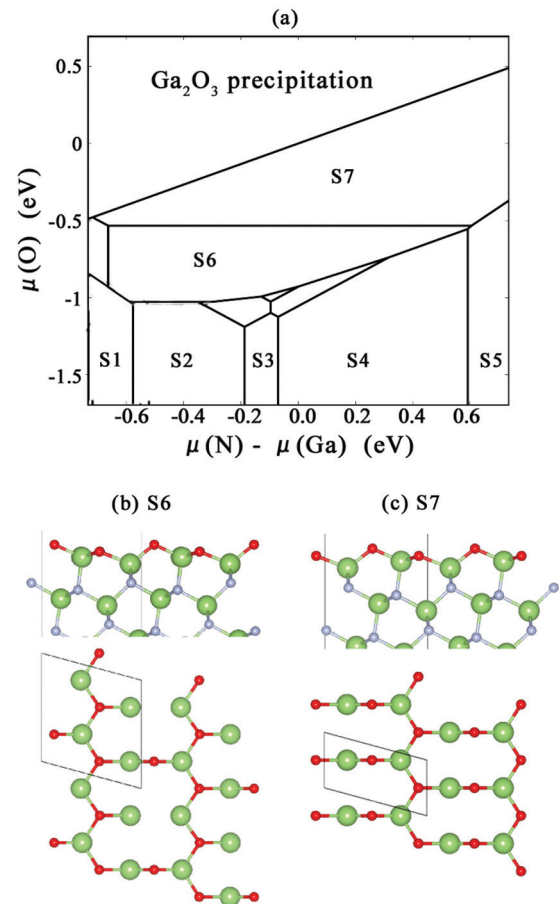

FIG. 7. (Color online) (a) Phase diagram of the GaN $(10\bar{1}1)$ surface with oxygen present up to 2×2 supercell reconstructions. Important reconstructions are labeled from S1 to S7. Structures S1 to S5 are shown in Fig. 6. Side views and top views of structures S6 and S7 are shown in (b) and (c). Large balls, gallium; small gray balls, nitrogen; small red balls, oxygen.

Ga_2O_3 solid:

$$2\mu(\text{O}) \leqslant G(\text{O}_2),$$
$$2\mu(\text{Ga}) + 3\mu(\text{O}) \leqslant G(\text{Ga}_2\text{O}_3), \quad (7)$$
$$x\mu(\text{Ga}) + y\mu(\text{O}) \leqslant G(\text{N}_x\text{O}_y).$$

Therefore, the convex hull has two dimensions in $n(\text{O})$ and $[n(\text{Ga}) - n(\text{N})]$. Figure 7(a) shows the two-dimensional phase diagram in space of $\mu(\text{O})$ and $[\mu(\text{N}) - \mu(\text{Ga})]$, transformed from the convex hull found in our EA search. The two additional major reconstructions are structures S6 and S7. Compared to the cleaved surface, structure S6 has half of the top N layer removed, and half of the top N and all of the second N layer replaced by O. Structure S7 has the top two N replaced by O. Similar reconstructions for the $(10\bar{1}1)$ surface have been reported.[49] These reconstructions are favored because of the strong Ga-O bond and the electron counting rule. For example, the simple cleaved surface has three nitrogen dangling bonds per surface cell. Because each N dangling bond needs 3/4 electron to become filled, the surface needs 9/4 electrons per surface unit cell to satisfy the electron counting rule. For structure

S7, substituting two N atoms with two O introduces two extra electrons, almost exactly satisfying the electron counting rule.

IV. CONCLUSIONS

In summary, we present a specially designed method to automatically explore low-energy surface reconstructions with variable surface atoms and reconstruction cells. The power of this approach is illustrated by application to diamond (100)/(111) surfaces. Applying it to MgO (111) and GaN-O (10$\bar{1}$1) surfaces, we find several additional low-energy reconstruction models. All of the systems investigated in this paper show quite complex surface reconstruction behaviors, indicating that an automated search of the potential energy landscape can be very helpful for us to understand surface chemistry. We demonstrate our method of predicting surface reconstruction based on an evolutionary approach can be generally applied to any binary and even multicomponent systems.

*qiang.zhu@stonybrook.edu

[1] Q.-K. Xue, Q. Z. Xue, R. Z. Bakhtizin, Y. Hasegawa, I. S. T. Tsong, T. Sakurai, and T. Ohno, Phys. Rev. Lett. **82**, 3074 (1999).

[2] A. Reinert, C. Payne, L. Wang, J. Ciston, Y. Zhu, and P. Khalifah, (unpublished). These authors identify the (10$\bar{1}$1) surface in powders of GaN/ZnO alloy, but say little about the structure of that surface.

[3] R. E. Schlier and H. E. Farnsworth, J. Chem. Phys. **30**, 917 (1959).

[4] K. Takayanagi, Y. Tanishiro, S. Takahashi, and M. Takahashi, Surf. Sci. **164**, 367 (1985).

[5] K. D. Brommer, M. Needels, B. E. Larson, and J. D. Joannopoulos, Phys. Rev. Lett. **68**, 1355 (1992).

[6] F. Chuang, C. Ciobanu, V. Shenoy, C. Wang, and K. Ho, Surf. Sci. **573**, L375 (2004).

[7] R. M. Briggs and C. V. Ciobanu, Phys. Rev. B **75**, 195415 (2007).

[8] D. Mei, L. Xu, and G. Henkelman, J. Phys. Chem. C **113**, 4522 (2009).

[9] M. Sierka, T. K. Todorova, J. Sauer, S. Kaya, D. Stacchiola, J. Weissenrieder, S. Shaikhutdinov, and H.-J. Freund, J. Chem. Phys. **126**, 234710 (2007).

[10] K. Reuter and M. Scheffler, Phys. Rev. Lett. **90**, 046103 (2003).

[11] A. R. Oganov and C. G. Glass, J. Chem. Phys. **124**, 244704 (2006).

[12] A. R. Oganov, A. O. Lyakhov, and M. Valle, Acc. Chem. Res. **44**, 227 (2011).

[13] Q. Zhu, A. R. Oganov, C. W. Glass, and H. T. Stokes, Acta Crystallogr., Sect. B: Struct. Sci. **68**, 215 (2012).

[14] A. O. Lyakhov, A. R. Oganov, H. T. Stokes, and Q. Zhu, Comput. Phys. Commun. **184**, 1172 (2013).

[15] A. O. Lyakhov, A. R. Oganov, and M. Valle, Comput. Phys. Commun. **181**, 1623 (2010).

[16] K. Li, X. Wang, F. Zhang, and D. Xue, Phys. Rev. Lett. **100**, 235504 (2008).

[17] A. O. Lyakhov and A. R. Oganov, Phys. Rev. B **84**, 092103 (2011).

[18] A. R. Oganov and M. Valle, J. Chem. Phys. **130**, 104504 (2009).

[19] G.-X. Qian, R. M. Martin, and D. J. Chadi, Phys. Rev. B **38**, 7649 (1988).

[20] J. C. Thomas, N. A. Modine, J. M. Millunchick, and A. Van der Ven, Phys. Rev. B **82**, 165434 (2010).

[21] W. Zhang *et al.*, arXiv:1211.3644.

[22] J. P. Perdew, K. Burke, and M. Ernzerhof, Phys. Rev. Lett. **77**, 3865 (1996).

[23] P. E. Blochl, Phys. Rev. B **50**, 17953 (1994).

[24] G. Kresse and J. Furthmüller, Phys. Rev. B **54**, 11169 (1996).

[25] K. Shiraishi, J. Phys. Soc. Jpn. **59**, 3455 (1990).

[26] J. Neugebauer and M. Scheffler, Phys. Rev. B **46**, 16067 (1992).

[27] G. Makov and M. C. Payne, Phys. Rev. B **51**, 4014 (1995).

[28] J. Ristein, Surf. Sci. **600**, 3677 (2006).

[29] D. W. Brenner, Phys. Rev. B **42**, 9458 (1990).

[30] J. Gale and A. Rohl, Mol. Simul. **29**, 291 (2003).

[31] K. C. Pandey, Phys. Rev. Lett. **47**, 1913 (1981).

[32] S. E. Boulfelfel, A. R. Oganov, and S. Leoni, Sci. Rep. **2**, 471 (2012).

[33] Y. Wang, J. E. Panzik, B. Kiefer, and K. K. M. Lee, Sci. Rep. **2**, 520 (2012).

[34] J. Ciston, A. Subramanian, and L. D. Marks, Phys. Rev. B **79**, 085421 (2009).

[35] J. Ciston, A. Subramanian, D. Kienzle, and L. Marks, Surf. Sci. **604**, 155 (2010).

[36] D. Wolf, Phys. Rev. Lett. **68**, 3315 (1992).

[37] F. Finocchi, A. Barbier, J. Jupille, and C. Noguera, Phys. Rev. Lett. **92**, 136101 (2004).

[38] R. Plass, K. Egan, C. Collazo-Davila, D. Grozea, E. Landree, L. D. Marks, and M. Gajdardziska-Josifovska, Phys. Rev. Lett. **81**, 4891 (1998).

[39] W.-B. Zhang and B.-Y. Tang, J. Phys. Chem. C **112**, 3327 (2008).

[40] Z. Wang, J. Bentley, E. Kenik, L. Horton, and R. McKee, Surf. Sci. **273**, 88 (1992).

[41] Q. Zhu, A. R. Oganov, and A. O. Lyakhov, Phys. Chem. Chem. Phys. **15**, 7696 (2013).

[42] T. A. Mellan and R. Grau-Crespo, J. Chem. Phys. **137**, 154706 (2012).

[43]T. Akiyama, D. Ammi, K. Nakamura, and T. Ito, Phys. Rev. B **81**, 245317 (2010).

[44]A. Garcia and J. E. Northrup, Appl. Phys. Lett. **65**, 708 (1994).

[45]M. D. Pashley, Phys. Rev. B **40**, 10481 (1989).

[46]S. B. Zhang and S.-H. Wei, Phys. Rev. Lett. **92**, 086102 (2004).

[47]L. Zhang, E. G. Wang, Q. K. Xue, S. B. Zhang, and Z. Zhang, Phys. Rev. Lett. **97**, 126103 (2006).

[48]W.-J. Lee and Y.-S. Kim, Phys. Rev. B **84**, 115318 (2011).

[49]J. E. Northrup, Phys. Rev. B **73**, 115304 (2006).